Low-Field MRI of Laser Polarized Noble Gas

C. H. Tseng,[1,2,3] G. P. Wong,[1] V. R. Pomeroy,[4] R. W. Mair,[1] D. P. Hinton,[5] D. Hoffmann,[1]
R. E. Stoner,[1] F. W. Hersman,[4] D. G. Cory,[3] and R. L. Walsworth[1]
[1]*Harvard-Smithsonian Center for Astrophysics, Cambridge, Massachusetts 02138*
[2]*Department of Radiology, Brigham and Women's Hospital, Boston, Massachusetts 02115*
[3]*Department of Nuclear Engineering, MIT, Cambridge, Massachusetts 02139*
[4]*Department of Physics, University of New Hampshire, Durham, New Hampshire 03824*
[5]*Massachusetts General Hospital, NMR Center, Charlestown, Massachusetts 02129*
(Received 27 April 1998)

NMR images of laser polarized ^{3}He gas were obtained at 21 G using a simple, homebuilt instrument. At such low fields magnetic resonance imaging (MRI) of thermally polarized samples (e.g., water) is not practical. Low-field noble gas MRI has novel scientific, engineering, and medical applications. Examples include portable systems for diagnosis of lung disease, as well as imaging of voids in porous media and within metallic systems. [S0031-9007(98)07442-0]

PACS numbers: 76.60.Pc, 32.80.Bx, 87.59.Pw, 87.62.+n

In this paper we demonstrate a powerful diagnostic technique: NMR imaging at low magnetic fields using laser polarized noble gas. Conventional magnetic resonance imaging (MRI) employs large magnetic fields ($\sim$1 T) to induce an observable thermal Boltzmann polarization in the nuclear spins of liquids such as water. MRI is a minimally invasive imaging technique with enormous impact in the biomedical and physical sciences. Examples include diagnostic clinical medicine [1], biological research, such as mapping of brain function [2], materials science (e.g., imaging the flow of shaken granular media [3]), and soft condensed matter physics, such as imaging the coarsening of foams [4]. Nevertheless, the large magnetic fields of conventional MRI require cumbersome and expensive equipment, and limit the technique's scientific and practical applications [5].

As demonstrated in this paper, the greatly increased nuclear spin polarization of the noble gases ^{3}He and ^{129}Xe, provided by optical pumping techniques ("laser polarization") [6], enables efficient gas-phase MRI at low magnetic fields ($\sim$10 G) using a simple, small, and inexpensive device. With this demonstration, the door is opened to a wide variety of new MRI applications. Examples in the biomedical field include portable systems for diagnostic lung imaging in humans [7], and low-cost tabletop MRI instruments for research in animals. Furthermore, a low-field noble gas MRI system would be compatible with operation in restricted environments, such as on board a space station, and may permit lung imaging of patients with artificial transplants such as pacemakers [8].

In the physical sciences, low-field noble gas MRI will be effective in imaging voids in two classes of materials that are problematic for high-field MRI: (i) heterogeneous systems, such as porous and granular media, which distort high-field images because of large, solid-gas magnetic susceptibility gradients; and (ii) electrical conductors, which prevent high-field MRI by Faraday (i.e., rf) shielding. Also, low-field NMR measurements of the restricted diffusion of noble gas imbibed in porous media (e.g., reservoir rock) may provide an effective and practical diagnostic of fluid permeability in such media.

At low magnetic fields and near room temperature, the thermally polarized nuclear magnetization of systems such as ^{1}H in water is extremely weak (spin polarizations $\sim 10^{-8}$), requiring extensive signal averaging in order to obtain a resolvable NMR signal, and making imaging impractical with conventional methods [5,9,10]. With laser polarization, however, angular momentum is transferred from photons to nuclei, and a large nonequilibrium nuclear spin polarization ($>10\%$) can be created in the spin-$\frac{1}{2}$ noble gases, ^{3}He and ^{129}Xe, independent of the applied magnetic field [6]. Laser polarized noble gas can be stored in specially prepared containers for several hours before the spin polarization decays back to thermal equilibrium. In "real world" samples such as biological tissue, air, and porous sandstone, the ^{3}He and ^{129}Xe spin polarization lifetime (T_1) is typically $\sim$10 s, still quite long for many purposes. Laser polarization greatly enhances the NMR detection sensitivity of the noble gases [11], enabling diverse applications such as gas-phase imaging at high magnetic fields (e.g., of the lung) [7], dissolved-state biomedical investigations [12], chemical physics and materials science studies [13], precision frequency measurements [14], and, as reported in this paper, practical MRI at low magnetic fields [15].

As a demonstration of low-field noble gas MRI, we imaged glass and plastic cells ("phantoms") containing laser polarized ^{3}He gas and thermally polarized water, at both high (4.7 T) and low (21 G) magnetic fields. Laser polarization of ^{3}He was accomplished with a standard spin-exchange optical pumping technique that employs Rb vapor as an intermediary to transfer angular momentum from laser photons to ^{3}He nuclear spins [6]. The ^{3}He glass cells were held in a static magnetic field of $\sim$100 G, heated

to ~170 °C in a hot air oven, and illuminated by 15 W of 795 nm light (~3 nm FWHM) from a fiber-coupled laser diode array (Optopower, Inc.). After about 3 hours of laser polarization, the ^{3}He phantoms were cooled to room temperature, walked over to the MRI instrument (without a holding magnetic field), and then placed in an appropriately tuned rf coil at the center of the low- or high-field MRI magnet. All ^{3}He phantoms contained 2.7 atm of ^{3}He, 100 torr of nitrogen, and a small amount of Rb metal, and were imaged with a ^{3}He spin polarization of ~10%.

MRI at 4.7 T was performed using a commercial GE Omega/CSI spectrometer/imager operating at 152 MHz for ^{3}He and 200 MHz for ^{1}H, while imaging at 21 G was performed with an inexpensive, homebuilt spectrometer/imager operating at 67 kHz for ^{3}He and 88 kHz for ^{1}H, and employing a simple, wire-wound solenoid electromagnet (see Fig. 1). (A detailed description of our low-field MRI system will be provided in a future paper. The solenoid design is described in [16].) All images were obtained without signal averaging using standard MRI techniques. For example, a spin echo pulse sequence was used for ^{1}H imaging of water phantoms at 4.7 T, and a low-flip-angle gradient echo technique (known as FLASH) was used for imaging the laser polarized ^{3}He gas phantoms [10]. (Low-flip-angle techniques are widely used for MRI of laser polarized noble gas because of the finite and difficult-to-replenish sample magnetization [7].) The low-field imaging employed magnetic field gradients up to 0.2 G/cm, chosen to keep field variations across the sample small relative to the main field of ~20 G, and hence to validate the secular approximation used to generate undistorted images from MRI data [17].

As shown in Fig. 2, low-field ^{3}He images have comparable spatial resolution to high-field images of water and ^{3}He. Not surprisingly, low-field water images could not be obtained due to the very small ^{1}H spin polarization at 21 G. Our prototype low-field MRI system provides ^{3}He images with a good, two-dimensional resolution of ~1 mm^2 for a data acquisition time of 10 s and a sample or slice thickness of ~1 cm. For example, the H-shaped ^{3}He image shown in Fig. 2d has a two dimensional resolution of 0.6 × 1.5 mm and a sample thickness of 21 mm. In contrast, using naive scaling laws, approximately *two months* of signal averaging would be needed to make an

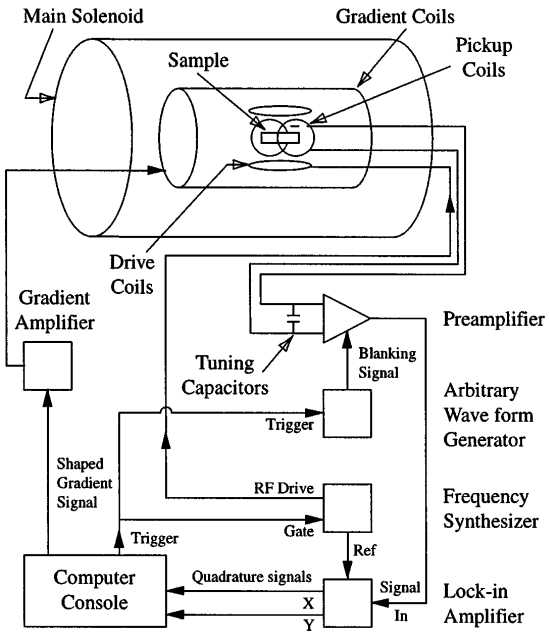

FIG. 1. Schematic of the homebuilt low-field MRI system. The main magnetic field (B_z) of ~20 G is created by an unshielded, copper wire solenoid. Gradient coils provide controllable, linear variations of B_z along the x, y, and z directions, which are necessary for imaging. Around the sample, coils tuned to the spins' Larmor frequency provide NMR excitation ("drive") and detect the resultant NMR signal ("pickup"). A frequency synthesizer operating close to the spins' Larmor frequency is gated by a millisecond TTL trigger to provide rf drive pulses. The pickup signal goes from a preamplifier—which is blanked during the drive pulse to avoid saturation—to a lock-in amplifier for phase-sensitive detection. A computer controls the magnetic field gradients and rf drive pulses, and performs data digitization and storage.

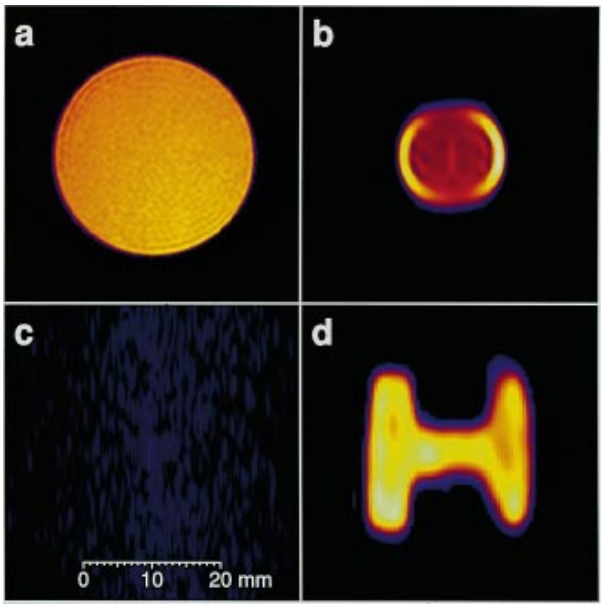

FIG. 2(color). Comparison of NMR images taken at 4.7 T and 21 G. Images at 4.7 T were obtained using a GE Omega/CSI spectrometer/imager: (a) Water inside a cylindrical Plexiglas cell; and (b) laser polarized ^{3}He gas inside a cylindrical glass cell (the increased signal intensity near the edges is due to restricted gas diffusion near the cell walls, i.e., edge enhancement [15]). Comparison images at 21 G were obtained using the homebuilt spectrometer/imager (see schematic in Fig. 1). (c) No image of water inside a cylindrical glass cell because of the very low ^{1}H spin polarization, but (d) a clear image of laser polarized ^{3}He gas inside a handblown, roughly H-shaped glass cell. All four images are to the same scale, as given in (b). The width and height of the gas space within the glass H cell are each 22 mm, and the thickness is 21 mm. The 21 G images were acquired in ~10 s using standard gradient echo imaging sequences.

^{1}H water image of comparable resolution at 21 G using our low-field MRI system.

We found that the signal-to-noise ratio of low-field, laser polarized noble gas MRI was sufficient that the limit to imaging resolution was set by gas diffusion [10]. Diffusion coefficients for gases are $\sim 10^4$ times larger than for liquids [18]. Therefore, significant gas atom displacement can occur during the application of the small imaging gradients that are appropriate for low-field MRI, limiting the image resolution [17]. For example, with a gradient echo imaging method, an imaging gradient of ~ 0.1 G/cm sets a diffusion-limited imaging resolution of ~ 1 mm for free ^{3}He gas at standard temperature and pressure (STP) [10]. Note that this imaging resolution can be improved by reducing the effective noble gas diffusion coefficient: e.g., in restricted environments (the lung, granular media, etc.), or in the presence of a buffer gas with a large scattering cross section.

An endemic problem in high-field MRI is spatial variations in magnetic susceptibility, for example, at the solid-gas or liquid-gas interfaces in granular media, foams, or the lung. Such susceptibility variations create local magnetic field gradients that induce both spatially homogeneous and inhomogeneous NMR line broadening at high magnetic fields: the homogeneous broadening reduces imaging resolution while the inhomogeneous broadening causes image distortion. Operating at low magnetic field greatly reduces these effects because the magnitude of susceptibility-induced local field gradients is proportional to the applied field. For example, we measured the NMR linewidth of laser polarized ^{3}He gas imbibed into rat lungs to be less than 3 Hz at 21 G, whereas recent measurements at high magnetic fields found much broader NMR linewidths ($\sim$100 Hz for ^{3}He gas imbibed into guinea pig lungs at 2 T and human lungs at 1.5 T [19]). The nonlinear nature of susceptibility-induced distortion is evident in the high-field water images shown in Figs. 3a and 3b, while the reduced susceptibility distortion of low-field noble gas MRI is clearly demonstrated in Figs. 3c and 3d. Similar susceptibility-induced problems also limit NMR diffusion measurements at high magnetic fields, where background gradients in heterogeneous samples can make experiments difficult or impossible [20]. Again, such problems should be greatly ameliorated with low-field noble gas operation,

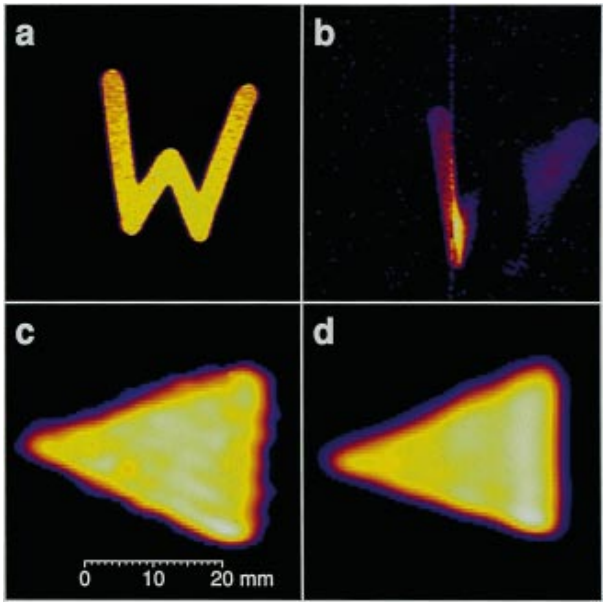

FIG. 3(color). Reduced magnetic susceptibility distortion at low magnetic fields. At 4.7 T, an NMR image of a water sample in a machined, W-shaped Plexiglas cell is (a) undistorted when no high magnetic susceptibility materials are nearby, but is (b) severely distorted by susceptibility-induced magnetic field gradients when placed next to four sealed tubes of paramagnetic materials (gadolinium chloride, nickel chloride, magnesium chloride, and gadopentetate dimeglumine). However, at 21 G an NMR image of laser polarized ^{3}He gas in a handblown, roughly triangular glass cell is undistorted both (c) without nearby paramagnetic materials and (d) when placed next to the same four tubes of paramagnetic materials that distorted the high-field water image in (b). The gas space within the triangular cell has a base length of 23.5 mm, equal side lengths of 34 mm, and a thickness of 23 mm.

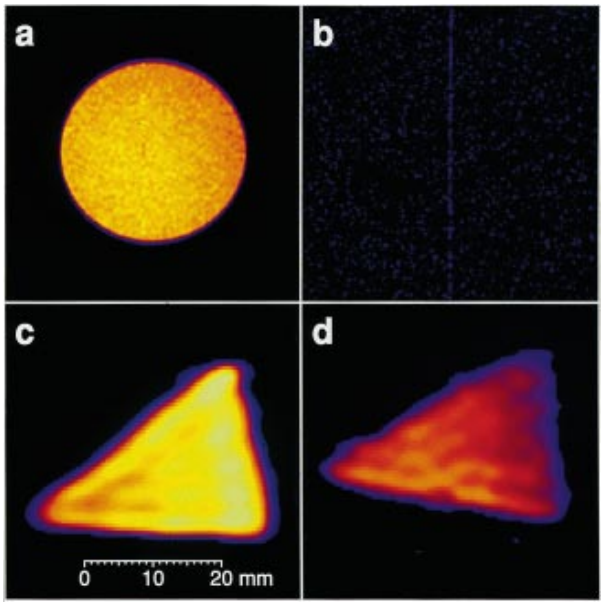

FIG. 4(color). Imaging of voids within a conductor. Samples of water and laser polarized ^{3}He gas were encased in identical rf shields made of 25 μm thick brass. The rf shield reduced the water NMR signal by 3 orders of magnitude at 4.7 T, but reduced the ^{3}He signal minimally at 21 G. This modest low-field signal reduction is consistent with reduced Faraday (i.e., rf) shielding of the NMR excitation pulses and signals at low magnetic fields. NMR imaging was performed at 4.7 T of (a) a cylindrical water sample, and (b) the same sample encased in the brass shield, illustrating the impracticality of imaging spaces within an electrical conductor at high magnetic fields. Comparison images were obtained successfully at 21 G of (c) laser polarized ^{3}He gas in a handblown, roughly triangular glass cell (the same cell as in Fig. 3), and (d) the triangular cell encased in the brass shield, demonstrating the utility of low-field noble gas MRI for imaging voids within conductively shielded objects.

providing a practical technique for measuring fluid permeability in porous media.

Low-field noble gas MRI can also examine voids inside electrically conducting materials. At the lower NMR frequencies enabled by low-field operation, RF electromagnetic fields can penetrate much deeper into conducting materials. Figure 4 demonstrates the ability of low-field noble gas MRI to image gas spaces within conductively shielded objects. This new technique may be useful in studies of fissures or cavities inside metals, for example, in aerospace components, or in measuring wall thinning of pipes in steam generation plants and elsewhere. Together, the efficacy of low-field noble gas MRI for both paramagnetic and metallic materials should allow imaging of interstitial spaces in a wide variety of granular media, and thus provide a powerful probe of three dimensional granular structure, dynamics, and relative grain-gas flow.

In summary, low-field noble gas MRI is a powerful diagnostic technique with novel applications in physical and biomedical science. We developed a simple low-field apparatus that provides laser polarized ^{3}He gas images at 21 G in a few seconds, with a two dimensional spatial resolution of ~ 1 mm^2 for a sample or slice thickness of ~ 1 cm, comparable to the resolution at high magnetic fields provided by commercial MRI instruments.

We gratefully acknowledge J. Moore for preparation of excised rat lungs. This work was supported by NSF Grant No. BES-9612237, NASA Grants No. NAGW-5025 and No. NAG5-4920, the Whitaker Foundation, and the Smithsonian Institution.

[1] P. G. Morris, *NMR Imaging in Biology and Medicine* (Clarendon, Oxford, 1986).

[2] S. A. Engel *et al.,* Nature (London) **369**, 525 (1994).

[3] E. E. Ehrichs *et al.,* Science **267**, 1632 (1995).

[4] C. P. Gonatas *et al.,* Phys. Rev. Lett. **75**, 573 (1995).

[5] Conventional MRI systems have been operated at magnetic fields as low as 160 G using a simple, low-cost electromagnet [see G. C. do Nascimento, R. E. de Souza, and M. Engelsberg, J. Phys. E **22**, 774 (1989); G. C. do Nascimento, M. Engelsberg, and R. E. de Souza, Measur. Sci. Tech. **3**, 370 (1992)]. However, the inherently low thermal spin polarization attainable at such magnetic fields leads to lower image resolution and greater data acquisition times, and is not feasible for gas-phase MRI without laser polarization.

[6] ^{3}He can be laser polarized using either of two techniques: spin-exchange optical pumping [see the recent review article T. G. Walker and W. Happer, Rev. Mod. Phys. **69**, 629 (1997)], or metastability exchange optical pumping [see, e.g., G. Eckert *et al.,* Nucl. Instrum. Methods Phys. Res., Sect. A **320**, 53 (1992)]. ^{129}Xe can be effectively laser polarized using only the first of these techniques. All optical pumping methods have their origin in the work of Kastler and co-workers in the 1950s [see the classic review article W. Happer, Rev. Mod. Phys. **44**, 169 (1972)].

[7] M. S. Albert *et al.,* Nature (London) **370**, 199 (1994); J. R. MacFall *et al.,* Radiology **200**, 553 (1996); M. Ebert *et al.,* Lancet **347**, 1297 (1996); P. Bachert *et al.,* Magn. Reson. Med. **36**, 192 (1996); H. U. Kauczor *et al.,* Radiology **201**, 564 (1996); J. P. Mugler *et al.,* Magn. Reson. Med. **37**, 809 (1997). Currently, laser polarized noble gas MRI is being tested as a diagnostic tool for chronic obstructive pulmonary disease (COPD), the fourth leading cause of death in the United States. The production of laser polarized noble gas is being commercialized [e.g., by Magnetic Imaging Technologies, Inc., 2500 Meridian Parkway, Suite 175, Durham, NC 27713].

[8] F. G. Shellock, S. Morisoli, and E. Kanal, Radiology **189**, 587 (1993).

[9] Y. S. Greenberg, Rev. Mod. Phys. **70**, 175 (1998).

[10] P. T. Callaghan, *Principles of Nuclear Magnetic Resonance Microscopy* (Clarendon, Oxford, 1991).

[11] R. D. Black *et al.,* Radiology **199**, 867 (1996).

[12] A. Bifone *et al.,* Proc. Natl. Acad. Sci. U.S.A. **93**, 12 932 (1996); S. Peled *et al.,* Magn. Reson. Med. **36**, 340 (1996); K. Sakai *et al.,* J. Magn. Reson. **111**, 300 (1996); M. E. Wagshul *et al.,* Magn. Reson. Med. **36**, 183 (1996); S. D. Swanson *et al.,* Magn. Reson. Med. **38**, 695 (1997); B. M. Goodson *et al.,* Proc. Natl. Acad. Sci. U.S.A. **94**, 14 725 (1997).

[13] D. Raftery *et al.,* Phys. Rev. Lett. **66**, 584 (1991); Y.-Q. Song *et al.,* J. Magn. Reson. A **115**, 127 (1995); G. Navon *et al.,* Science **271**, 1848 (1996); K. L. Sauer, R. J. Fitzgerald, and W. Happer, Chem. Phys. Lett. **277**, 153 (1997).

[14] T. E. Chupp, R. J. Hoare, R. L. Walsworth, and B. Wu, Phys. Rev. Lett. **72**, 2363 (1994); R. E. Stoner *et al.,* Phys. Rev. Lett. **77**, 3971 (1996); D. Bear *et al.,* Phys. Rev. A **57**, 5006 (1998).

[15] Researchers at Princeton have previously reported 1D low-field NMR images of laser polarized ^{3}He gas: B. Saam, N. Drukker, and W. Happer, Chem. Phys. Lett. **263**, 481 (1996). Also, scientists in France are pursuing MRI of laser polarized ^{3}He in human lungs at 0.1 T: L. Darrasse, G. Guillot, P.-J. Nacher, and G. Tastevin, C.R. Acad. Sci. Paris, Ser. IIb **324**, 691 (1997); L. Darrasse, G. Guillot, P.-J. Nacher, and G. Tastevin, Proc. Int. Soc. Magn. Reson. Meet., 6th Meeting, 449 (1998).

[16] R. J. Hanson and F. M. Pipkin, Rev. Sci. Instrum. **36**, 179 (1965).

[17] J. M. Blackledge, *Quantitative Coherent Imaging* (Academic Press, London, 1989); P. T. Callaghan and C. D. Eccles, J. Magn. Reson. **78**, 1 (1988).

[18] For example, at room temperature the molecular diffusion coefficient of liquid water is 1.7×10^{-5} cm^2 s^{-1}, while at room temperature and one atmosphere the xenon gas self-diffusion is 5.7×10^{-2} cm^2 s^{-1} and the ^{3}He gas self-diffusion coefficient is 1.8 cm^2 s^{-1}.

[19] R. Surkau *et al.,* Proc. Int. Soc. Magn. Res. Meet. 5th Meeting, 182 (1997); X. J. Chen *et al.,* Proc. Int. Soc. Magn. Res. Meet. 5th Meeting, 2108 (1997).

[20] L. L. Latour, L. Li, and C. H. Sotak, J. Magn. Reson. B **101**, 72 (1993).